Experimental and Analytical Characterization of Time-Variant V2V Channels in a Highway Scenario

Gerd Sommerkorn[1], Martin Käske[1],
Daniel Czaniera[1], Christian Schneider[1],
Giovanni Del Galdo[1] and Reiner S. Thomä[1]
[1]Institute for Information Technology
Technische Universität Ilmenau
D-98684 Ilmenau, Germany
Email: som@tu-ilmenau.de

Michael Walter[2]
[2]Institute of Communications and Navigation
German Aerospace Center (DLR)
D-82234 Wessling, Germany
Email: m.walter@dlr.de

***Abstract*—The time-variant characteristic of the vehicle to vehicle channel is discussed using measurements at 2.53 GHz from a highway scenario. For typical use cases, spectrograms in the time-delay as well as the Doppler domain are shown based on sequences of the generalized local scattering function. Delay-Doppler-bounds to be expected for single bounce reflections are determined by known movements of the transmitter and receiver using a channel representation in a prolate spheroidal coordinate system. Dominant moving scatterers are identified by visual inspection using proper meta data.**

Keywords – V2V, channel sounding, local scattering function, highway scenario, prolate spheroidal coordinates, Doppler limits

I. Introduction

Vehicle to everything (V2X) communications are currently under active investigation to enable intelligent transport systems (ITS) covering improved safety and environmentally friendly driving to enable ever more advanced use cases, ranging from platooning, emergency lane change, overtaking assistance, to sensor sharing [1]–[3], ultimately leading to cooperative automated driving.

Because these use cases demand in parallel low latency and high reliability, V2X is one of the most challenging *verticals* that 5G networks are aiming to support. V2X channels exhibit unique properties that strongly differ from cellular wireless networks due to the highly dynamic environment including frequent blockage, low rise antennas, fast changing multi-link properties a.s.o., which require detailed understanding for channel modelling based on measurements. Hence, the vehicular communication channel is characterized by a non-stationary fading process [4]–[6] and the wide-sense stationary uncorrelated scattering (WSSUS) assumption, which is a very popular and simplified description of random linear time-varying channels, is not exactly satisfied within this context [5]. Therefore, we consider the generalized local scattering function (GLSF), which is derived for analyzing non-WSSUS channels [5], [7], [8]. Based on this method delay and Doppler spectra can be estimated.

In this paper, we give a brief outline of a new channel sounding campaign for vehicle to vehicle (V2V) use cases in a highway scenario. The delay and Doppler domains have been analyzed using sequences of the GLSF, whereby contributions of dominant stationary and moving SXs have been identified and brought in accordance with their theoretical Doppler limits using the prolate spheroidal coordinate system (PSCS).

TABLE I
Measurement System

Channel Sounder	RUSK (MEDAV GmbH)
Transmit signal & power	multi tone @40 dBm
Bandwidth & center frequency	20 MHz @ 2.53 GHz
Channel impulse response length	6.4 μs
MIMO snapshot rate	2.6 kHz
MIMO sub-channels	5x5 (#Tx x #Rx) w/o guard
AGC switching	within MIMO sub-channels
Metadata	GPS and 360°-Video

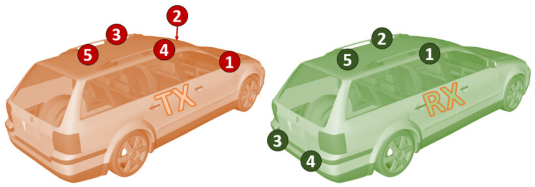

Fig. 1 Antenna placement on transmitter- and receiver car.

II. Measurement Campaign

The multiple input multiple output (MIMO) measurement campaign was performed nearby Ilmenau (Germany) using a RUSK channel sounder operating at 2.53 GHz and focusing on V2V applications. The transmitter as well as the receiver have been mounted into two station wagons that were moving on a highway. Both cars have been equipped with five distributed application antennas mounted on the roofs and bumpers.

A sketch of the respective locations of the antennas can be seen in Fig. 1. All but the antennas 3 and 4 on the receiver (RX) car are magnetic mounted MGD-2400-5500 (*MobileMark*) whose principal radiation pattern (measured without the influence of the car body) is depicted in Fig. 2. Antennas 3 and 4 of the RX car are patch antennas integrated into the rear bumper of the car.

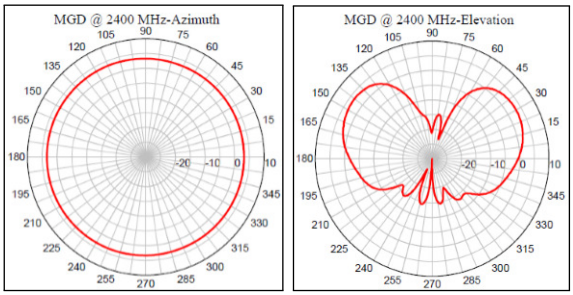

(a) Azimuth (b) Elevation

Fig. 2 Azimuth- and elevation-cut of magnetic mount antennas at 2.4 GHz (*MGD-2400-5500*).

In addition, GPS loggers and 360° cameras were installed to log the locations of the cars and the traffic conditions around them. Several maneuvers have been carried out, representing multiple use cases like drive in convoy or oncoming traffic and overtaking.

Table I summarizes the measurement setup.

III. Processing

A. Generalized Local Scattering Function

The well-known set of Bello-functions [9] can be used to characterize random linear time-variant channels. Here, the so called scattering function (SF), is of high significance, since the power delay profile (PDP) as well as the power Doppler profile (PDoP) can directly be derived from it. Nevertheless, the SF requires the channel to fulfill the wide sense stationary (WSS) and uncorrelated scattering (US) assumptions [10].

To overcome that, for non-WSSUS channels such as the V2X channel, [10] introduced the GLSF. It can be interpreted as a time- & frequency-variant SF and is computed via a 2-D Fourier transform from short time and frequency intervals of the two-dimensional time-variant transfer function (TF). The approach using the GLSF can be thought of as segmenting the whole sequence of measurements into blocks that fulfill the WSSUS assumption *locally*. In order to obtain a reliable estimation from these short intervals, a multi-taper approach is suggested in [10]. The main idea within this methodology is to use orthogonal window functions to extract a number of independent ensembles from the same process. These ensembles are averaged to lower the variance of the resulting estimate. Using this approach, the GLSF is defined as

$$\widetilde{C}_h(t,f;f_D,\tau) = E\left\{\sum_{k=0}^{K-1}\gamma_k|S^{G_k}(t,f;f_D,\tau)|^2\right\} \quad (1)$$

where

$$S^{G_k}(t,f;f_D,\tau) = \mathrm{e}^{j2\pi f\tau}\iint H(t',f') G_k^*(t'-t,f'-f)\mathrm{e}^{-j2\pi(f_D\Delta t'-\tau f')}\mathrm{d}t'\mathrm{d}f'. \quad (2)$$

The coefficients must fulfill $\sum_{k=1}^{K}\gamma_k = 1$. Furthermore, the filter function $G_k(t,f)$ can be expressed as

$$G_k(t,f) = g_i(t)g_j(f) \quad (3)$$

with g_i ($i = 0..I-1$) and g_j ($j = 0..J-1$) being the window functions, and I and J being the number of window functions in time and frequency domain, respectively. Furthermore $K = I\cdot J$ is the number of overall window functions and $k = i\cdot J+j$ is the respective index.

As appropriate window functions, discrete prolate spheroidal sequences (DPSSs) are proposed in [11] and applied in [12] and [13]. These sequences, defined in [14], are orthogonal to each other, while being strictly limited in time or frequency domain and having a high energetic concentration in the respective other domain.

B. Processing Scheme

To calculate the GLSFs from the TF the lengths of the used DPSSs in time and frequency domain have to be chosen. These lengths need to be short enough, such that the channel can be expected to be quasi-WSSUS within the resulting regions. An approach to estimate these minimal stationarity intervals is proposed in [11]. Applying it to the measurements summarized in Section II, a length of 19.8 ms (equal to 52 consecutive MIMO snapshots) in time domain and a length of 18.75 MHz (corresponding to 121 frequency bins) in frequency domain would result. Here, for the following analysis results a length of the sequences in the frequency domain has been set to 129 frequency bins corresponding to the full bandwidth of the measurements. Consequently it is assumed that the channel is stationary over the observed frequency range. Concerning the length of the sequences in the time domain, a reasonable approach would be to round up to the next power of 2, which leads to 64 snapshots. For the sake of an improved Doppler resolution, we considered using 128. Doubling the used snapshots did not result in any observable effects that could stem from a possible violation of the found minimum stationarity. Thus, all presented results are obtained using a window length of 128 snapshots in time domain. Furthermore, the numbers of DPSSs in time and frequency domain have been set to $I = J = 2$. The GLSFs are calculated in steps of 16 MIMO snapshots corresponding to an overlap of 87.5 %. The computed time-varying GLSFs have been used to derive PDoPs and PDPs.

IV. Limiting Frequencies

From the experimental results it was found that the PDoPs are almost always limited by a certain highest Doppler frequency. This is expected since the Doppler frequency is naturally limited by the velocity and relative position of the RX, transmitter (TX) and scatterers (SXs). From the theory presented in [15] the limiting frequencies induced by single bounce SXs can be predicted using only the velocity vectors of RX, TX and SXs. There, the Doppler frequency is transformed into prolate spheroidal coordinates, which is more suitable to mathematically treat the problem [16]. The parameters ξ, η, and ϑ of the PSCS denote possible locations of a SX relative

to the locations of RX and TX. After transforming the Doppler frequency into the PSCS, we obtain

$$
\begin{aligned}
&f_{\mathrm{D}}\left(t;\xi,\eta,\vartheta\right) = \qquad (4)\\
&= \Bigg(\frac{\sqrt{\left(\xi^2-1\right)\left(1-\eta^2\right)}}{\xi+\eta}\Big(\left(v_{x_{\mathrm{TX}}}+v_{z_{\mathrm{SX}}}\right)\cos\vartheta\\
&+\left(v_{y_{\mathrm{TX}}}+v_{y_{\mathrm{SX}}}\right)\sin\vartheta\Big)+\frac{\sqrt{\left(\xi^2-1\right)\left(1-\eta^2\right)}}{\xi-\eta}\Big(\\
&\quad\left(v_{x_{\mathrm{RX}}}+v_{x_{\mathrm{SX}}}\right)\cos\vartheta+\left(v_{y_{\mathrm{RX}}}+v_{y_{\mathrm{SX}}}\right)\sin\vartheta\Big)\\
&+\frac{\xi\eta+1}{\xi+\eta}\left(v_{z_{\mathrm{TX}}}+v_{z_{\mathrm{SX}}}\right)+\frac{\xi\eta-1}{\xi-\eta}\left(v_{z_{\mathrm{RX}}}+v_{z_{\mathrm{SX}}}\right)\Bigg)\frac{f_{\mathrm{c}}}{c}\,.
\end{aligned}
$$

Note that the Doppler frequency is a function of time due to time-dependency of the Cartesian components of the velocity vectors $\mathbf{v}_{\mathrm{TX}} = [v_{x_{\mathrm{TX}}}, v_{y_{\mathrm{TX}}}, v_{z_{\mathrm{TX}}}]^{\mathrm{T}}$, $\mathbf{v}_{\mathrm{RX}} = [v_{x_{\mathrm{RX}}}, v_{y_{\mathrm{RX}}}, v_{z_{\mathrm{RX}}}]^{\mathrm{T}}$, and $\mathbf{v}_{\mathrm{SX}} = [v_{x_{\mathrm{SX}}}, v_{y_{\mathrm{SX}}}, v_{z_{\mathrm{SX}}}]^{\mathrm{T}}$ of TX, RX, and SX, respectively. The Doppler frequency for the 2D V2V channel is calculated by using $\vartheta \in \{0, \pi\}$, which corresponds to a horizontal plane.

By using the theory of algebraic curves [17], a closed-form solution for the limiting frequencies of the spectrum can be deduced as shown in [15]. The limiting frequencies can be calculated by solving the sixth degree polynomial $g(\eta)$, which is given by

$$
g(\eta) = a_6\eta^6 + a_5\eta^5 + a_4\eta^4 + a_3\eta^3 + a_2\eta^2 + a_1\eta + a_0\,, \quad (5)
$$

with coefficients[1] a_i, $i = 0, \ldots, 6$ given by (6).

Since $g(\eta) = 0$ can have up to six real solutions, we will only use the solutions that provide the maximum and minimum frequency in order to bound the spectrum caused by stationary and moving SXs. Poles within the spectrum are out of the scope of this paper.

For distances (from TX to SX to RX) close to the line of sight (LOS), e.g., $\xi \to 1$, the limiting frequencies simplify and we obtain the following frequencies:

$$
\begin{aligned}
f_{1,2}(t) &= \frac{\pm\|\mathbf{v}_{\mathrm{TX}}+\mathbf{v}_{\mathrm{SX}}\| - \left(v_{z_{\mathrm{RX}}}+v_{z_{\mathrm{SX}}}\right)}{c} f_{\mathrm{c}}\\
f_{3,4}(t) &= \frac{\pm\|\mathbf{v}_{\mathrm{RX}}+\mathbf{v}_{\mathrm{SX}}\| + \left(v_{z_{\mathrm{TX}}}+v_{z_{\mathrm{SX}}}\right)}{c} f_{\mathrm{c}}\,. \qquad (7)
\end{aligned}
$$

From the four obtained frequencies, we select the maximum and minimum frequency in order to bound the spectrum.

The calculated frequencies can be observed both in Fig. 3 and 5. For the use case, where both vehicles drive in the same direction (*convoy*), the limiting frequencies do not change over delay and time. This means that the limiting frequency is a horizontal line, see Fig. 3. For the *opposite* use case, the limiting frequencies are *not* constant over delay, so the spectral width changes over delay and time.

To illustrate the limiting Doppler frequency further, we calculated the Doppler frequencies in Table II, Table III and Table IV for the different scenarios. In order to simplify (7), we assumed that TX, RX, and SX are aligned along the z-axis. The result is shown below the tables.

[1]Due to space constraints we assumed $\mathbf{v}_{\mathrm{SX}} = 0$ for the coefficients.

TABLE II
SX BEHIND TX AND RX (f_{c}=2.53 GHz)

use case	$v_{z_{\mathrm{TX}}}$	$v_{z_{\mathrm{RX}}}$	$v_{z_{\mathrm{SX}}}$	f_{D}
opposite	$100\,\mathrm{km\,h^{-1}}$	$-100\,\mathrm{km\,h^{-1}}$	$-100\,\mathrm{km\,h^{-1}}$	-469 Hz
			$0\,\mathrm{km\,h^{-1}}$	0 Hz
			$100\,\mathrm{km\,h^{-1}}$	469 Hz
convoy	$100\,\mathrm{km\,h^{-1}}$	$100\,\mathrm{km\,h^{-1}}$	$-100\,\mathrm{km\,h^{-1}}$	-937 Hz
			$0\,\mathrm{km\,h^{-1}}$	-469 Hz
			$100\,\mathrm{km\,h^{-1}}$	0 Hz

$f_{\mathrm{D}} = +\left(\left(v_{z_{\mathrm{SX}}} - v_{z_{\mathrm{TX}}}\right) + \left(v_{z_{\mathrm{SX}}} - v_{z_{\mathrm{RX}}}\right)\right)\frac{f_{\mathrm{c}}}{c}$

TABLE III
SX BETWEEN TX AND RX (f_{c}=2.53 GHz)

use case	$v_{z_{\mathrm{TX}}}$	$v_{z_{\mathrm{RX}}}$	$v_{z_{\mathrm{SX}}}$	f_{D}
opposite	$100\,\mathrm{km\,h^{-1}}$	$-100\,\mathrm{km\,h^{-1}}$	$-100\,\mathrm{km\,h^{-1}}$	469 Hz
			$0\,\mathrm{km\,h^{-1}}$	469 Hz
			$100\,\mathrm{km\,h^{-1}}$	469 Hz
convoy	$100\,\mathrm{km\,h^{-1}}$	$100\,\mathrm{km\,h^{-1}}$	$-100\,\mathrm{km\,h^{-1}}$	0 Hz
			$0\,\mathrm{km\,h^{-1}}$	0 Hz
			$100\,\mathrm{km\,h^{-1}}$	0 Hz

$f_{\mathrm{D}} = -\left(\left(v_{z_{\mathrm{SX}}} - v_{z_{\mathrm{TX}}}\right) - \left(v_{z_{\mathrm{SX}}} - v_{z_{\mathrm{RX}}}\right)\right)\frac{f_{\mathrm{c}}}{c}$

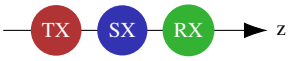

V. Results

The processing scheme outlined in Section III has been applied to the measurements resulting in time-varying and MIMO-channel-selective GLSFs. Furthermore, the discussed limiting frequencies for stationary and moving SXs have been determined using the positions of TX and RX during the measurement runs.

A. Use case *convoy*

In the example shown in Fig. 3, TX and RX moved in the same direction, with a driving speed of $\approx$100 $\mathrm{km\,h^{-1}}$, respectively

TABLE IV
SX BEFORE TX AND RX (f_{c}=2.53 GHz)

use case	$v_{z_{\mathrm{TX}}}$	$v_{z_{\mathrm{RX}}}$	$v_{z_{\mathrm{SX}}}$	f_{D}
opposite	$100\,\mathrm{km\,h^{-1}}$	$-100\,\mathrm{km\,h^{-1}}$	$-100\,\mathrm{km\,h^{-1}}$	469 Hz
			$0\,\mathrm{km\,h^{-1}}$	0 Hz
			$100\,\mathrm{km\,h^{-1}}$	-469 Hz
convoy	$100\,\mathrm{km\,h^{-1}}$	$100\,\mathrm{km\,h^{-1}}$	$-100\,\mathrm{km\,h^{-1}}$	937 Hz
			$0\,\mathrm{km\,h^{-1}}$	469 Hz
			$100\,\mathrm{km\,h^{-1}}$	0 Hz

$f_{\mathrm{D}} = -\left(\left(v_{z_{\mathrm{SX}}} - v_{z_{\mathrm{TX}}}\right) + \left(v_{z_{\mathrm{SX}}} - v_{z_{\mathrm{RX}}}\right)\right)\frac{f_{\mathrm{c}}}{c}$

$$
\begin{aligned}
a_0 =& \left(\left(v_{x_{\mathrm{TX}}} - v_{x_{\mathrm{RX}}}\right)^2 + \left(v_{z_{\mathrm{TX}}} + v_{z_{\mathrm{RX}}}\right)^2 \right) \xi^4 - \left(v_{z_{\mathrm{TX}}} + v_{z_{\mathrm{RX}}}\right)^2 \xi^6 \\
a_1 =& 4 \left({v_{x_{\mathrm{RX}}}}^2 - {v_{x_{\mathrm{TX}}}}^2 + {v_{z_{\mathrm{RX}}}}^2 - {v_{z_{\mathrm{TX}}}}^2 \right) \xi^3 + 2 \left({v_{x_{\mathrm{TX}}}}^2 - {v_{x_{\mathrm{RX}}}}^2 + 2 \left({v_{z_{\mathrm{TX}}}}^2 - {v_{z_{\mathrm{RX}}}}^2 \right) \right) \xi^5 \\
a_2 =& \left(6 \left({v_{x_{\mathrm{TX}}}}^2 + {v_{x_{\mathrm{RX}}}}^2 + {v_{z_{\mathrm{TX}}}}^2 + {v_{z_{\mathrm{RX}}}}^2 \right) + 4 \left(v_{x_{\mathrm{TX}}} v_{x_{\mathrm{RX}}} - v_{z_{\mathrm{TX}}} v_{z_{\mathrm{RX}}} \right) \right) \xi^2 \\
& + \left(2 v_{z_{\mathrm{TX}}} v_{z_{\mathrm{RX}}} - 8 \left({v_{x_{\mathrm{TX}}}}^2 + {v_{x_{\mathrm{RX}}}}^2 \right) - 7 \left({v_{z_{\mathrm{TX}}}}^2 + {v_{z_{\mathrm{RX}}}}^2 \right) \right) \xi^4 + \left(\left(v_{x_{\mathrm{TX}}} + v_{x_{\mathrm{RX}}}\right)^2 + \left(v_{z_{\mathrm{TX}}} + v_{z_{\mathrm{RX}}}\right)^2 \right) \xi^6 \\
a_3 =& 4 \left({v_{x_{\mathrm{RX}}}}^2 - {v_{x_{\mathrm{TX}}}}^2 + {v_{z_{\mathrm{RX}}}}^2 - {v_{z_{\mathrm{TX}}}}^2 \right) \xi + 4 \left(3 \left({v_{x_{\mathrm{TX}}}}^2 - {v_{x_{\mathrm{RX}}}}^2 \right) + 2 \left({v_{z_{\mathrm{TX}}}}^2 - {v_{z_{\mathrm{RX}}}}^2 \right) \right) \xi^3 \\
& + 4 \left({v_{x_{\mathrm{RX}}}}^2 - {v_{x_{\mathrm{TX}}}}^2 + {v_{z_{\mathrm{RX}}}}^2 - {v_{z_{\mathrm{TX}}}}^2 \right) \xi^5 \\
a_4 =& \left(v_{x_{\mathrm{TX}}} - v_{x_{\mathrm{RX}}}\right)^2 + \left(v_{z_{\mathrm{TX}}} + v_{z_{\mathrm{RX}}}\right)^2 + \left(2 v_{z_{\mathrm{TX}}} v_{z_{\mathrm{RX}}} - 8 \left({v_{x_{\mathrm{TX}}}}^2 + {v_{x_{\mathrm{RX}}}}^2 \right) - 7 \left({v_{z_{\mathrm{TX}}}}^2 + {v_{z_{\mathrm{RX}}}}^2 \right) \right) \xi^2 \\
& + \left(6 \left({v_{x_{\mathrm{TX}}}}^2 + {v_{x_{\mathrm{RX}}}}^2 + {v_{z_{\mathrm{TX}}}}^2 + {v_{z_{\mathrm{RX}}}}^2 \right) - 4 \left(v_{x_{\mathrm{TX}}} v_{x_{\mathrm{RX}}} + v_{z_{\mathrm{TX}}} v_{z_{\mathrm{RX}}} \right) \right) \xi^4 \\
a_5 =& 2 \left({v_{x_{\mathrm{TX}}}}^2 - {v_{x_{\mathrm{RX}}}}^2 + 2 \left({v_{z_{\mathrm{TX}}}}^2 - {v_{z_{\mathrm{RX}}}}^2 \right) \right) \xi + 4 \left({v_{x_{\mathrm{RX}}}}^2 - {v_{x_{\mathrm{TX}}}}^2 + {v_{z_{\mathrm{RX}}}}^2 - {v_{z_{\mathrm{TX}}}}^2 \right) \xi^3 \\
a_6 =& - \left(v_{z_{\mathrm{TX}}} + v_{z_{\mathrm{RX}}}\right)^2 + \left(\left(v_{x_{\mathrm{TX}}} + v_{x_{\mathrm{RX}}}\right)^2 + \left(v_{z_{\mathrm{TX}}} + v_{z_{\mathrm{RX}}}\right)^2 \right) \xi^2 .
\end{aligned} \tag{6}
$$

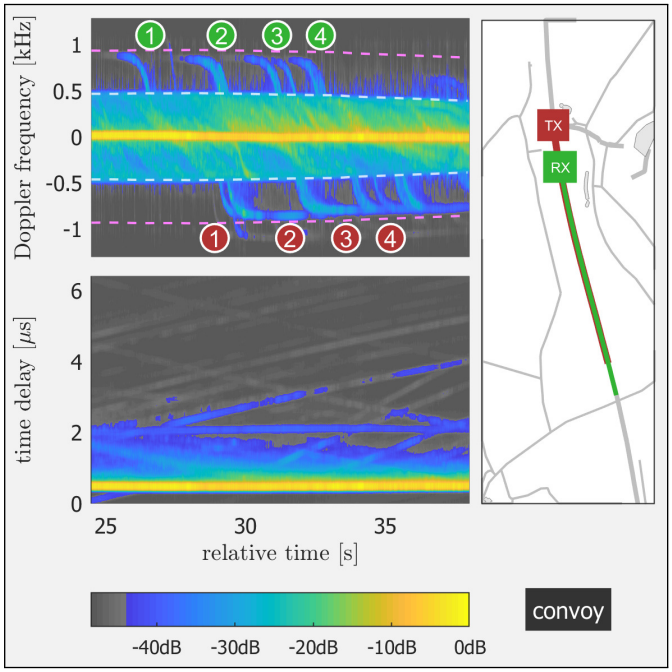

Fig. 3 Time-varying PDoP and PDP, TX and RX drive at a constant distance, one behind the other; dashed lines denote Doppler limits for stationary (white, $v_{z_{\mathrm{SX}}} = 0\,\mathrm{km\,h^{-1}}$) and mobile (magenta, $v_{z_{\mathrm{SX}}} = 100\,\mathrm{km\,h^{-1}}$) SXs; 4 trucks in oncoming direction (see Fig. 4)

Fig. 4 TX and RX drive at a constant distance, one behind the other, 4 trucks in oncoming direction (see Fig. 3)

Due to the almost constant distance between TX and RX the LOS path and close to LOS paths (caused by stationary and moving SXs) have no Doppler shifts (compare Table III). As soon as stationary SXs exist in front of and behind the convoy of TX and RX, characteristic edges in the PDoP occur at $\approx \pm 500\,\mathrm{Hz}$, which coincide perfectly with the white dashed lines plotted in Fig. 3. These lines are based on the positions of TX and RX and represent the expected limiting frequencies. Mobile SXs with $v_{z_{\mathrm{SX}}} = 100\,\mathrm{km\,h^{-1}}$ are drawn by magenta dashed lines at $\approx \pm 1\,\mathrm{kHz}$. Positive Doppler shifts in that range represent mostly the oncoming traffic before TX and RX (compare Table IV), while negative Doppler shifts correspond mostly to the traffic behind TX and RX (compare Table II).

Interestingly, in the PDoP shown in Fig. 3, four contributions can be seen which begin with a high positive Doppler shift, then appear to move to 0 Hz, and after some time recur and move to a high negative Doppler shift.

From the recorded videos we could identify four trucks passing on the opposite lane. The time stamp when the Doppler shift of a single component starts to go to 0 Hz corresponds to the time stamp when the RX is passing the truck. In similar fashion the Doppler shift starts to go to negative values as soon as the TX (driving behind the RX) is also passing the truck. Fig. 4 shows the views for all four trucks at different time stamps seen from the RX and the TX, respectively. The green and red numbered markers sync the movie frames to the time-varying PDoP and PDP depicted in Fig. 3.

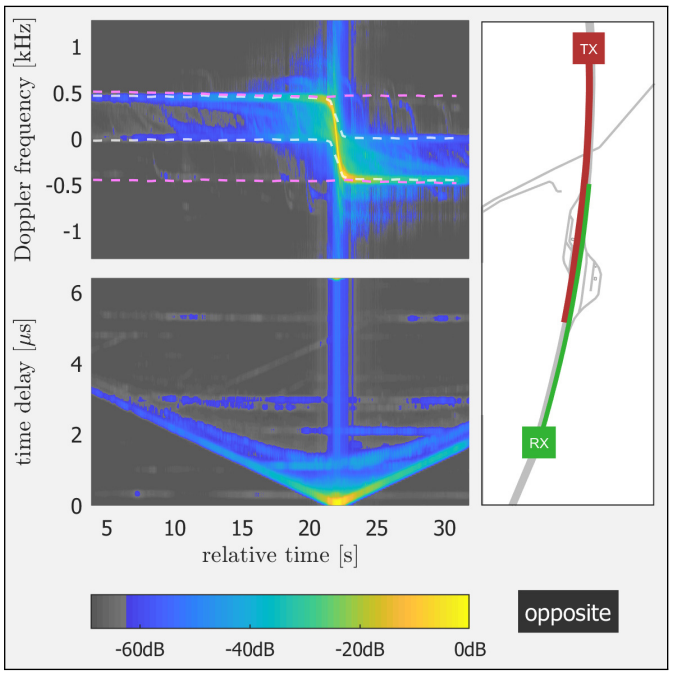

Fig. 5 Time-varying PDoP and PDP, TX and RX moving with same velocity in opposite directions (remark: too strong signal level during over ride); dashed lines denote Doppler limits for stationary (white, $v_{z_{\mathrm{SX}}} = 0\,\mathrm{km\,h^{-1}}$) and mobile (magenta, $v_{z_{\mathrm{SX}}} = 100\,\mathrm{km\,h^{-1}}$) SXs

B. Use case *opposite*

Here, both cars drove in opposite directions with a speed of $\approx$100 km h^{-1}, respectively. Prior to the moment of passing of the TX and RX, stationary SXs contribute Doppler shifts in a range of $\approx$0 Hz to 500 Hz. While SXs before or behind the TX and RX do not introduce Doppler shifts (see Section IV), stationary SXs in between both cars induce the maximum Doppler shift. After the passing the resulting Doppler shifts are negated.

In case of mobile SXs with a driving speed of $v_{z_{\mathrm{SX}}} = 100\,\mathrm{km\,h^{-1}}$ Doppler shifts of $\approx \pm 500$ Hz have to be expected dependent on the position and driving direction of the SX.

VI. Summary

In this paper results have been presented discussing V2V measurements and analysis in a highway scenario. For the analysis the GLSF has been chosen to extract the characteristics of the measurements in the Doppler and time-delay domain. We found characteristical *edges* in the PDoP that appear to be predominantly caused by LOS and fixed scatterers such as bridges or traffic signs. Doppler limits have been determined solving a sixth degree polynomial based on parameters of the PSCS helping to associate observed Doppler shifts with single-bounce reflections from both moving or stationary SXs. We found a good agreement between the analytically predicted limits in Doppler frequency and the experimental results. Furthermore, the evolution of scatterers as they pass or are passed by the measurement vehicles could be explained. In addition we were able to identify contributions from trucks moving in the oncoming traffic.

Acknowledgments

The authors would like to thank Huawei Technologies Düsseldorf GmbH, German Research Center Munich, for supporting this work and the Thüringer Innovationszentrum Mobilität (ThIMo), the VISTA4F ProExellenz research group funded by the Thüringer Ministerium für Wirtschaft, Wissenschaft und Digitale Gesellschaft as well as the research group "ELVIS" funded by the European Social Fund (ESF) under the grant 2015 FGR 0088.

References

[1] 3GPP, "Study on enhancement of 3GPP support for 5G V2X services (Release 15)," 3rd Generation Partnership Project (3GPP), techreport 3GPP TR 22.886 v15.1.0, Mar. 2017. [Online]. Available: http://www.3gpp.org

[2] IEEE, "Wireless LAN Medium Access Control (MAC) and Physical Layer (PHY) Specifications: Amendment 6: Wireless Access in Vehicular Environments," Institute of Electrical and Electronics Engineers (IEEE), techreport IEEE P802.11p: Part 11:, Jul. 2010. [Online]. Available: http://www.ieee.org

[3] 3GPP, "Study on channel model for frequencies from 0.5 to 100 GHz," 3rd Generation Partnership Project (3GPP), techreport 3GPP TR 38.901 V14.0.0, March 2017. [Online]. Available: http://www.3gpp.org

[4] A. F. Molisch, F. Tufvesson, J. Karedal, and C. F. Mecklenbrauker, "A survey on vehicle-to-vehicle propagation channels," *IEEE Wireless Communications*, vol. 16, no. 6, pp. 12–22, December 2009.

[5] G. Matz, "On non-wssus wireless fading channels," *IEEE Transactions on Wireless Communications*, vol. 4, no. 5, pp. 2465–2478, Sept 2005.

[6] T. J. Willink, "Wide-sense stationarity of mobile mimo radio channels," *IEEE Transactions on Vehicular Technology*, vol. 57, no. 2, pp. 704–714, March 2008.

[7] A. Paier, T. Zemen, L. Bernado, G. Matz, J. Karedal, N. Czink, C. Dumard, F. Tufvesson, A. F. Molisch, and C. F. Mecklenbrauker, "Non-wssus vehicular channel characterization in highway and urban scenarios at 5.2ghz using the local scattering function," in *2008 International ITG Workshop on Smart Antennas*, Feb 2008, pp. 9–15.

[8] L. Bernado, T. Zemen, A. Paier, J. Karedal, and B. H. Fleury, "Parametrization of the local scattering function estimator for vehicular-to-vehicular channels," in *2009 IEEE 70th Vehicular Technology Conference Fall*, Sept 2009, pp. 1–5.

[9] P. Bello, "Characterization of randomly time-variant linear channels," *IEEE Transactions on Communications Systems*, vol. 11, no. 4, pp. 360–393, December 1963.

[10] G. Matz, "On non-wssus wireless fading channels," *IEEE Transactions on Wireless Communications*, vol. 4, no. 5, pp. 2465–2478, Sept 2005.

[11] ——, "Doubly underspread non-wssus channels: analysis and estimation of channel statistics," in *2003 4th IEEE Workshop on Signal Processing Advances in Wireless Communications - SPAWC 2003 (IEEE Cat. No.03EX689)*, June 2003, pp. 190–194.

[12] A. Paier, T. Zemen, L. Bernado, G. Matz, J. Karedal, N. Czink, C. Dumard, F. Tufvesson, A. F. Molisch, and C. F. Mecklenbrauker, "Non-wssus vehicular channel characterization in highway and urban scenarios at 5.2ghz using the local scattering function," in *2008 International ITG Workshop on Smart Antennas*, Feb 2008, pp. 9–15.

[13] A. Ispas, G. Ascheid, C. Schneider, and R. Thoma, "Analysis of local quasi-stationarity regions in an urban macrocell scenario," in *2010 IEEE 71st Vehicular Technology Conference*, May 2010, pp. 1–5.

[14] D. Slepian, "Prolate spheroidal wave functions, fourier analysis, and uncertainty - v: The discrete case," *Bell System Technical Journal*, vol. 57, no. 5, pp. 1371–1430, May-June 1978.

[15] M. Walter, D. Shutin, and A. Dammann, "Algebraic analysis of the poles in the doppler spectrum for vehicle-to-vehicle channels," *IEEE Wireless Communications Letters*, vol. 7, no. 4, pp. 662–665, Aug 2018.

[16] M. Walter, D. Shutin, and U. Fiebig, "Prolate spheroidal coordinates for modeling mobile-to-mobile channels," *IEEE Antennas and Wireless Propagation Letters*, vol. 14, pp. 155–158, 2015.

[17] H. Hilton, *Plane algebraic curves*. The Clarendon press, 1920.